

# Chapter 19. Antarctic Sea Ice and Icebergs

**Robert G. Onstott**

General Dynamics - Advanced Information Systems, Ann Arbor, MI, USA

## 19.1 Introduction

The monitoring of floating ice in the Southern Ocean is of great interest because of its vast winter extent and the scale of its retreat during summer. With a winter extent that is about 20% greater than that in the Northern Hemisphere, Southern Ocean sea ice plays an important role in the global energy balance. In addition, the icebergs that calve from the Antarctic ice shelves and glacier tongues may initially be the size of a small state (e.g., 400 to 11,000 km<sup>2</sup>), and, frequently produce many smaller icebergs that may become deadly marine hazards. Icebergs are also a source of fresh water to the world's oceans.

There are important differences between the northern and southern polar oceans that affect sea ice conditions, and sea ice physical and microwave properties. In the Southern Ocean, sea ice is bounded on the south by the Antarctic continent, whereas to the north there is no land boundary. Ice formation regions extend north from the Antarctic coastline for hundreds of kilometers. In addition, the ocean around the Antarctic continent is essentially obstruction-free for hundreds of kilometers beyond the ice edge. Storms are frequent in the Southern Hemisphere and swell waves of significant height form in the open ocean and propagate into the Antarctic sea ice zone. Katabatic winds form because cold and dense air is pulled from high elevations to the coast by gravity. These winds flow off of this very cold continent over the ocean surface, are very strong, and may persist for long periods (e.g., days). These winds produce a dynamic ocean environment. Sea ice may be cleared from the coastline, enabling the production of new ice. In summary, the Southern Ocean is a very dynamic environment; wave conditions and storm frequency play a major role in determining sea ice physical and microwave properties.

Because of a dynamic oceanographic and atmospheric environment, ice concentration in the Antarctic is lower than that observed in the Arctic, at about 80% in winter, and 50% in summer, on average [Zwally *et al.*, 1983]. The maximum ice extent is observed in September, the minimum extent in February. The austral summer begins in December and ends in March. The Southern Ocean ice coverage has a maximum winter extent on the order of  $20 \times 10^6$  km<sup>2</sup> and a summer minimum on the order of  $4 \times 10^6$  km<sup>2</sup> (about three times the size of the U.S.), a summer retreat factor of about 5. Hence, the sea ice cover is primarily seasonal, and first year ice is the predominant ice form [Zwally *et al.*, 1983].

Discussion of the microwave remote sensing of floating ice in the Southern Ocean is presented in this chapter. Specific topics include the observation of sea ice, landfast ice, and icebergs. Regional ice characteristics, sea ice zones, and the expected seasonal backscatter response are discussed. Synthetic aperture radar (SAR) images are used to illustrate signature differences between ice forms and convergence/divergence features.

For an additional discussion of sea ice behavior, see Chapter 3, "SAR Measurements of Sea Ice." Discussion of the operational use of SAR is found in Chapter 20, "Operational Uses of SAR for Ice Classification and Analysis."

TABLE 19.1. Major Regional Characteristics in Influencing Ice Cover

Area Name	Sector	Characteristic
Weddell Sea	60°W to 20°E	Relatively cold ocean water influenced by large-scale cyclonic gyre and topographic barrier of the Antarctic Peninsula. Sea ice is compact. Large area of ice cover remains during the summer. A polynya forms occasionally.
Indian Ocean	20°E to 90°E	Ice edge retreats completely to the coast in several locations during summer.
Pacific Ocean	90°E to 160°E	Ice edge retreats completely to the coast in several locations during summer.
Ross Sea	160°E to 130°W	Relatively cold water and cyclonic circulation gyre influences open water formation near Ross Ice Shelf.
Bellingshausen – Amundsen Sea	130°W to 60°W	There is strong stratification of the open ocean water; this contributes to the retention of an extensive summer ice cover.

## 19.2 Critical Solid Ocean Features in the Southern Ocean

In the Southern Ocean, frozen seawater and fresh water are of great interest, as is the case in the Arctic, because of their areal extent and impact on the earth's climate. Sea ice is found around the full perimeter of Antarctica. It may be landfast, consolidated as floes in the ice pack, or a loose mixture of open water, frazil ice, and pancakes at the ice margins. Freshwater ice features are also numerous, and in the form of giant-to-small icebergs and bergy bits (large pieces of a glacier with between 100 and 300 m<sup>2</sup> of ice above the water line). Other features worthy of note include ice shelves, and glaciers that protrude far away from the coastline known as ice tongues. Glaciers may be floating on seawater or grounded on the seafloor.

## 19.3 Regional Characteristics and Sea Ice Zones

The region in which sea ice forms determines its winter properties and the likelihood of survival during summer. In addition, where the ice is located relative to the coastline and the open ocean boundary also affects its physical and electrical properties.

### 19.3.1 Regional Characteristics

The extent of Antarctica and the locations of the various seas in the Southern Ocean is shown in Figure 19.1. Ocean circulation around the continent and topographic barriers (e.g., Antarctic Peninsula and ice tongues) affects the sea ice cover through the stratification of the ocean water column and the formation of relatively cold ocean water. These effects determine whether polynyas (non-linear shaped openings enclosed in ice) form during winter, the quantity of ice retained during summer, and if the ice edge retreats completely to the coast. In addition, the very cold, high-velocity katabatic winds play a major role in (a) clearing ice from the coastline while facilitating rapid ice formation, (b) sweeping the air-ocean free of frazil ice, and (c) promoting high ice production during storms of long duration. The geographic

## Antarctic Sea Ice and Icebergs

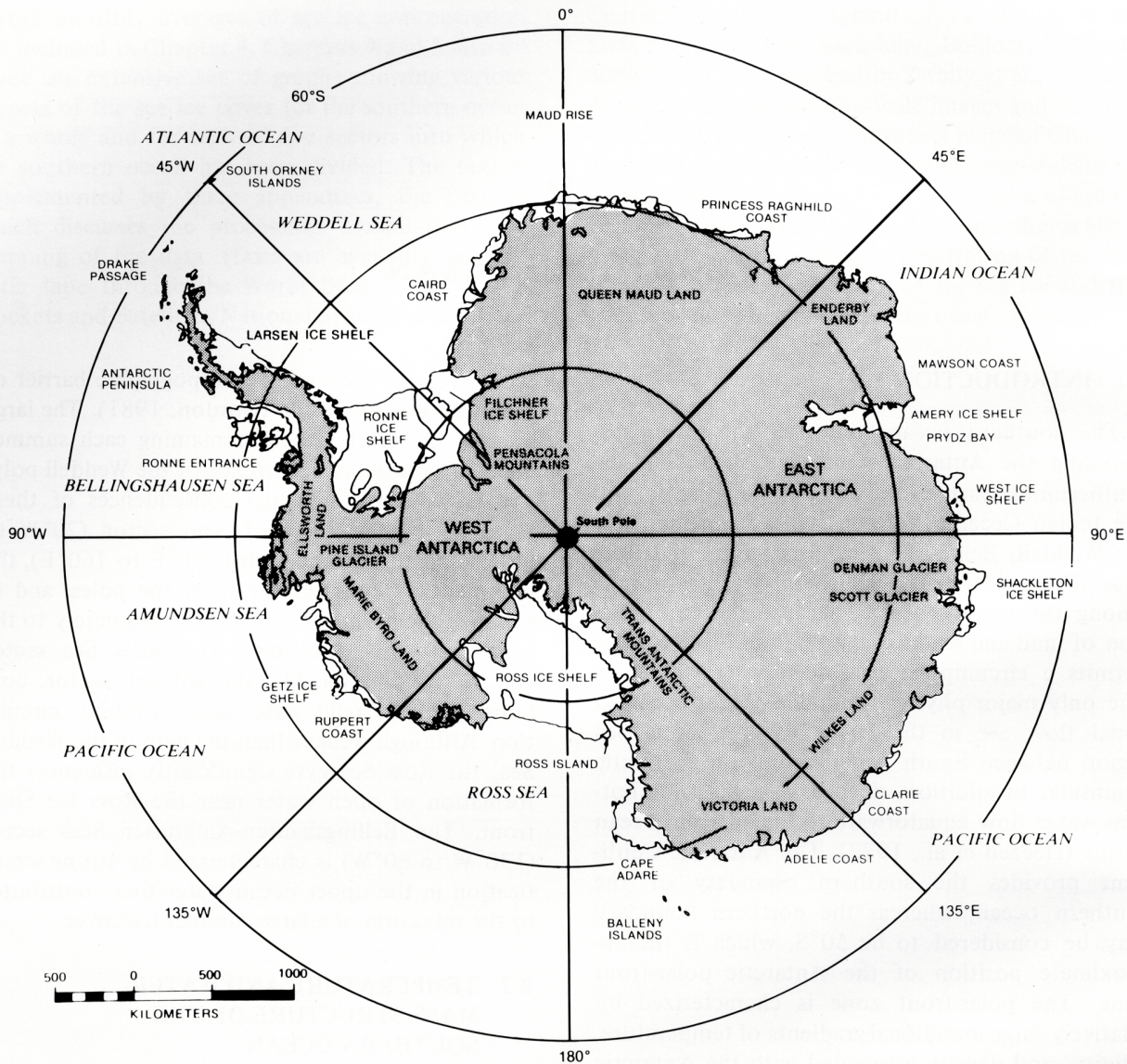


Figure 19.1. Map of the Antarctic and Southern Ocean showing the locations of the various seas and ice shelves [Zwally *et al.*, 1983].

sectors in which the various seas and oceans are contained and the characteristics of these regions are summarized in Table 19.1 [Zwally *et al.*, 1983].

### 19.3.2 Major Ice Zones

There are three primary ice zones around the Antarctic continent: (a) coastal, (b) pack, and (c) marginal. In the coastal zone, the ice is consolidated, and is often the oldest and thickest. Given the katabatic winds that flow off the continent over the ice-covered ocean, ice conditions even in the coastal regions will be dynamic during high wind episodes. Movement or shearing of the consolidated ice about the coastline produces near shore leads and the production of new ice, and the formation of pressure ridges and rubble areas. Polynyas may also form near the coast due to upwelling.

The predominant ice production zone is the marginal ice zone (MIZ) and is located immediately adjacent to the open ocean. In this zone, new ice is produced, formed into cakes and small floes several meters in diameter, and is dispersed among open water, grease ice, slush, and frazil. Ice in this region is greatly influenced by swell waves. The effects of swell include limiting the maximum diameter of a floe, the rafting of pans and floes upon one another, the piling of slush along floe boundaries, and the flooding of floes with seawater. Expected ice forms in this region include the full range of new and young sea ice categories: frazil, grease, pancake, grey, and grey-white. There will also be prominent bands of open water. Because of the young age of the ice, the snow cover is limited. SAR ice signatures in this region are prone to be modified by the surface flooding caused by swell and waves. An additional discussion of processes that occur at the ice edge is found in Chapter 18, "Processes at the Ice Edge - The Arctic."

Ice in the zone between the coastal and marginal ice zones is consolidated and is referred to as pack ice. Typically, ice floes are rougher, thicker, and stronger than ice in the other two regions. Because the ice is days to many weeks older, the snow cover is thicker than that found in the marginal ice zone. Because the ice is physically more stable, the SAR ice signatures in this region are also more stable than those found in the marginal ice zone. Storms, however, can affect ice signatures in this region because of rafting and flooding. Rafting adds more freeboard and may produce an increase in backscatter intensity. Divergence in this region will occur and cause the ice to break apart and form leads and polynyas. The predominant ice type in this region is first year with a heavy snow cover. When flooding of first year ice is limited to seawater accumulation at the snow-ice interface, the backscatter intensity is increased because the high dielectric constant of seawater and the spatially variable wicking of brine into the snow pack produces a dielectrically rough surface. However, if the entire snow pack is moistened because of the flooding event, the backscatter intensity may stay the same or even decrease. This wide range of backscatter values for the same ice type makes ice type and form discrimination difficult in the Antarctic.

#### 19.4 Sea and Fresh Water Ice General Characteristics

Before proceeding further, it is important to review some of the general characteristics of sea and fresh water ice that are found around Antarctica. Short descriptions of each of the various ice forms and some of their unique characteristics follow. An extensive discussion of Antarctic and Arctic sea ice physical properties and general characteristics is found in *Gow and Tucker* [1990].

- *New and Flooded Ice* is produced in significant quantities during winter, during and after episodes of high winds and waves that cause divergence in the ice fields or when the snow load becomes too great for a given ice thickness. The physical, electrical, and microwave properties of new and young sea ice are nearly identical to those found in the Arctic. This observation is based on (a) the examination of salinity, density, and ice fabrics, and (b) the similarity in the backscatter signatures in both the Arctic and Antarctic.
- *First Year Ice* has a thickness on the order of 0.7 m for level ice [*Wadhams et al.*, 1987], and on the order of 1 m for deformed ice [*Lange and Eicken*, 1991]. Snow cover is observed to be in the range from 5 to 30 cm. Ice and snow densities are similar to those of Arctic first year ice.
- *Second-Year or Multiyear Ice* has survived the summer melt. Most old Antarctic ice is in its second year. During summer, much of the ice in the Southern Ocean is advected into warmer

## Antarctic Sea Ice and Icebergs

water where it experiences significant melt. In-situ observations of second year and multiyear ice in the Antarctic are limited, but indicate a high likelihood of ice in the thickness range from 1 m to greater than 2 m and a heavy snow cover. A mean snow thickness as great as 0.75 m has been observed. Snow cover may become heavy enough to move the ice-snow interface to a position below sea level. Flooding of the snow-ice interface has been frequently observed for old ice, even though in-situ observation opportunities have been limited. Flooding of first year ice is also a common occurrence.

- *Snow* in the Antarctic is more abundant than in the Arctic, and snow depths are greater [Barry, 1989]. Snow properties in the Antarctic are similar to those found in the Arctic in terms of its ice crystal size distribution and snow pack density.
- *Deformed Ice* is found as pancake rims, rafted ice, or pressure ridges. Pressure ridge heights are smaller than those observed in the Arctic. The largest ridge heights or sails are on the order of 1 m [Weeks *et al.*, 1989, Lytle and Ackley, 1991]. In comparison, ridge heights in the Arctic of 2 to 4 m are common.
- *Icebergs* are composed of fresh water ice and are produced when sections of ice shelves or glacier tongues break off and become free floating. The detection of iceberg activity is of national interest because of the desire to monitor the “calving” rate and because of the great concern about icebergs entering shipping lanes and the serious hazard they pose for mariners. Icebergs in the Southern Oceans can be quite large.
- *Floating Glacier Tongues* are floating extensions of grounded ice sheets. Glaciers are composed of fresh water ice and form by the accumulation of snow.

### 19.5 Expected Backscatter Response and Seasonal Response

The discussion of the microwave response of Antarctic sea ice is separated according to ice type, and includes new, young, first-year, second-year, and multiyear ice.

#### 19.5.1 New/Young

SAR signatures of new, grease, frazil, slush, pancake, nilas, grey, and grey-white ice, and open water signatures are similar to those observed in the Arctic. These are the predominant signatures of the MIZ. The key difference between the MIZ in the Arctic and Antarctic is not a difference in backscatter level, but that the MIZ in the Antarctic covers a much more extensive area. Sea ice has a salinity in the range from 14 to about 5 part per thousand (ppt), whereas the surrounding sea water will have a salinity from 32 to 35 ppt.

#### 19.5.2 First Year Ice

A high proportion of first year ice in Antarctica has its origins as frazil and pancake ice rather than ice grown under quiescent conditions that produces congelation ice with a smooth snow-ice interface. The greater surface roughness of Antarctic ice increases its backscatter levels. Since first year ice often has a heavy snow load, flooding of the snow-ice interface occurs frequently [Ackley *et al.*, 1980]. An increase in the backscatter level is expected. The mixing of flooded with unflooded floes in a region produces a diverse range of radar signatures.

### 19.5.3 Second Year and Multiyear Ice

There is no distinct large area microwave SAR signature for multiyear ice in the Southern Ocean that compares to that observed in the Arctic. In addition, neither passive microwave nor microwave scatterometer observations which are global and frequent show such a unique multiyear ice signature [Gloersen *et al.*, 1992, Drinkwater, 1998a, Morris *et al.*, 1998]. Passive microwave imaging of the Antarctic does show a continuum of ice signatures. Note that the natural emission at microwave frequencies responds to the same physical and electrical properties that SAR responds to, but to different degrees. Since the thickness of old ice is on the order of 2 m and typically has a heavy snow cover that promotes flooding, the thickness and age of this ice form is masked. The current hypothesis is that pack ice experiences only one melt season before drifting into regions of high oceanic heat-flux where it melts. Using C-band SAR imagery, second-year and multiyear signatures are found to be indistinguishable from those for rough, first-year ice [Drinkwater, 2000].

### 19.5.4 Icebergs and Ice Sheets

Sources of iceberg and ice sheet backscatter signatures breakdown into three important categories: (a) very thick layers of snow and firn, (b) glacial ice with a thin snow layer, and (c) topography, such as crevasses, streamlines, and ice blocks. Layers of snow and firn, tens of meters thick, produce strong backscatter levels, because the particles act as discrete electromagnetic scatterers. The penetration at microwave wavelengths into low loss materials such as this is tens of meters. The scattering cross-section for each snow or firn particle may be very small, but the backscatter response is due to the accumulation of contributions over the depth that the radar signal penetrates. Glacial ice, however, has a very high density and a limited number of very small bubbles, and produces weak backscatter. Surface topography produces an enhanced backscatter because of dihedral or facet scattering back to the radar. When tall enough, topography may also produce radar shadow effects that work to highlight the topographical features.

### 19.5.5 Winter Backscatter Statistics

Example backscatter statistics for the Weddell Sea derived from space-borne SAR (ESA ERS-1) and spaceborne scatterometer (ESA ERS-1/2 Escat) are shown in Tables 2 and 3. For ERS-1, the mean backscatter winter response for first year and multiyear ice ranges from about  $-6$  to  $-16$  dB, about a 10 dB dynamic range. These values are 2-3 dB higher than those for similar ice forms observed in the Arctic and are attributable to a thicker snow layer, contribution from flooded ice floes, and rougher ice surfaces. The scatterometer data are also included here to document the range of backscatter levels observed and their association with ice type. New and young ice produce weak backscatter until deformed. As an example, the change of new ice into pancake ice produces a dramatic change in backscatter behavior (e.g., an increase of 14-20 dB) as seen in Table 3.

### 19.5.6 Summer Signatures

During the transition from winter to summer, scattering coefficients for the various sea ice forms converge to a cross-section of about  $-7.5$  dB, a signature that is similar to that of second-year and multiyear ice during winter [Drinkwater, 1998b]. This appears to be determined by two

## Antarctic Sea Ice and Icebergs

TABLE 19.2. Example Backscatter Statistics from ERS-1 (C-band, VV) SAR Imagery Collected at  $\approx 20^\circ$  Incident Angle in the Weddell Sea during July 1992 [*Drinkwater*, 1998a].

Ice Type	Mean (dB)	STD (dB)
Smooth FY	-15.5 to -16.1	$\pm 1.0$
Rough FY	-9.5 to -10.1	$\pm 1.8$
SY & MY	-5.7 to -6.8	$\pm 2.3$

Table 19.3. Example Backscatter Statistics from Winter (C-band VV) Escat Data Collected at  $40^\circ$  Incident Angle in the Weddell Sea during February 1992 [*Drinkwater*, 1998a].

Ice Type	Mean (dB)	STD (dB)
New & Young	-32.0 to -20.0	--
Smooth FY	-20.0 to -14.0	$\pm 1.5$
Rough FY	-14.0 to -11.0	$\pm 2.0$
MY & Pancakes	-11.0 to -6.0	$\pm 3.0$
Icebergs	-6.0 to 0.0	$\pm 2.3$

primary effects. One is associated with the flooding of the ice-water interface with seawater, and the second is associated with surface melting effects. Air temperatures rise above  $0^\circ\text{C}$  only briefly during the Antarctic summer. Because of cool temperatures and heavy snow covers, surface melting is limited and snow is retained on sea ice throughout the summer. Melt pool development in the Antarctic is not widely observed. In addition, with limited free water production and percolation of fresh water through a floe's vertical structure, ice floes experience little desalination during summer and maintain a salinity profile like that of first-year ice. A key characteristic of Antarctic sea ice is that summer surface melting is short-lived. The summer backscatter response is characterized by large fluctuations in cross-section that are correlated with melt and freeze cycles [*Drinkwater and Lytle*, 1997; *Drinkwater*, 2000]. Melt and freeze cycles are often associated with the propagation of weather systems through a region and will cause the snow pack to moisten, thereby reducing backscatter levels. The combination of high ocean heat flux and summer short-wave radiation absorbed by the ocean surface (in small lead fractions) rapidly disposes of most of the summer sea ice cover by promoting melting at the ice-water interfaces (e.g., sides and bottom) [*Ackley*, 1987].

### 19.6 SAR Observations of Antarctic Sea Ice

The first space-based radar observations of the Antarctic were conducted by the Shuttle Imaging Radar (SIR-B) mission in 1984 [*Carsey et al.*, 1986; *Martin et al.*, 1987]. SIR-B flew on 5 October 1998 and was able to map 15 million square kilometers of the world's oceans and landmasses during its 16-hour mission. The European Space Agency ERS-1 SAR was

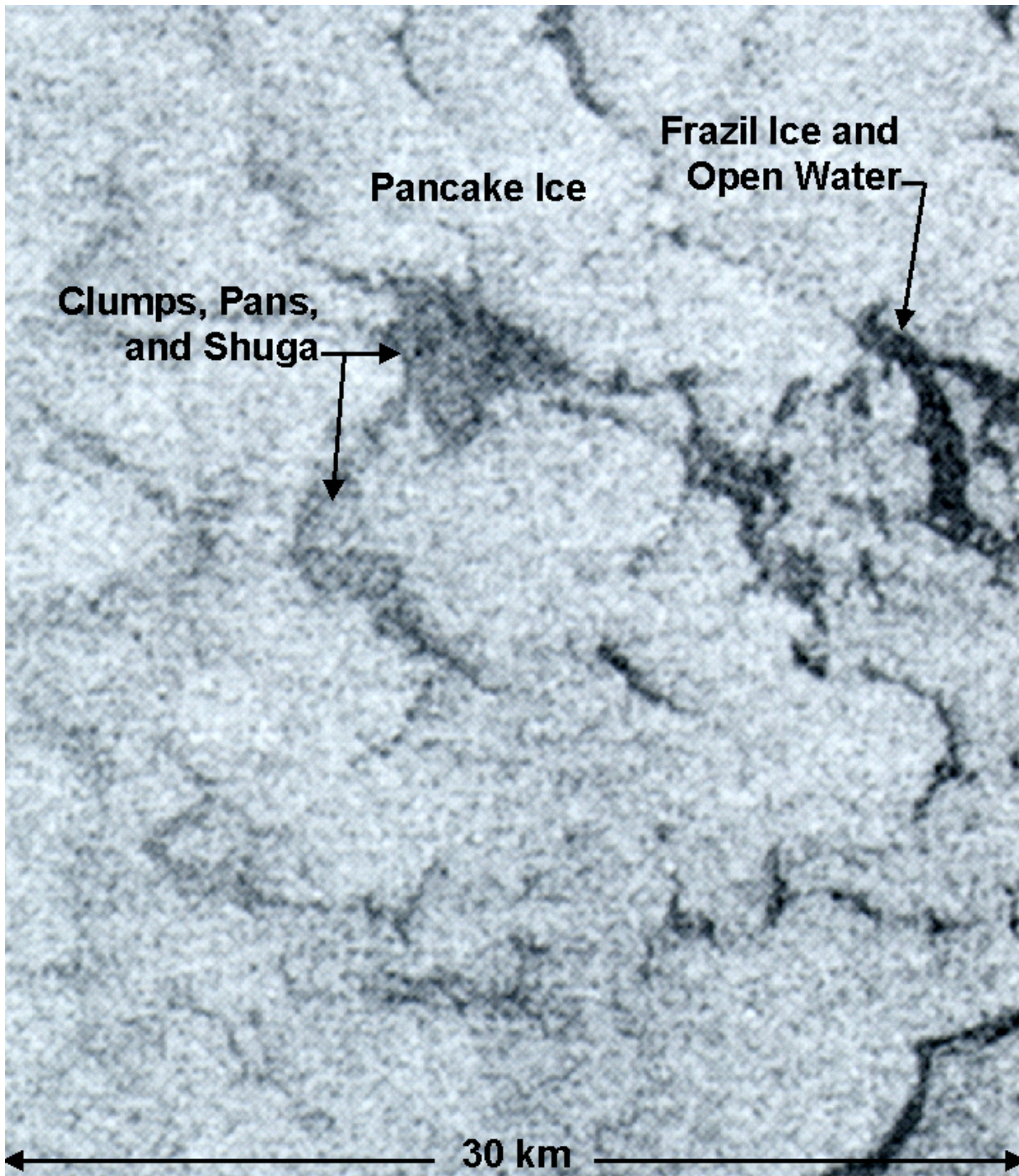


Figure 19.2. SIR-B (L-band, HH) image of frazil and pancake ice found in the Scotia Sea during October 1984. Image location is 56°S 29°W.

launched in 1991 and was used to obtain the first detailed observations of the radar backscatter of sea ice in the Antarctic. The launch of the Canadian Space Agency RADARSAT-1 in 1995 further improved the frequency of coverage. The full mapping of the continent and the measurement of velocity for fast moving glaciers has been provided by two dedicated RADARSAT-1 Antarctic Mapping Missions in 1997 (AMM-1) and 2001 (AMM-2).

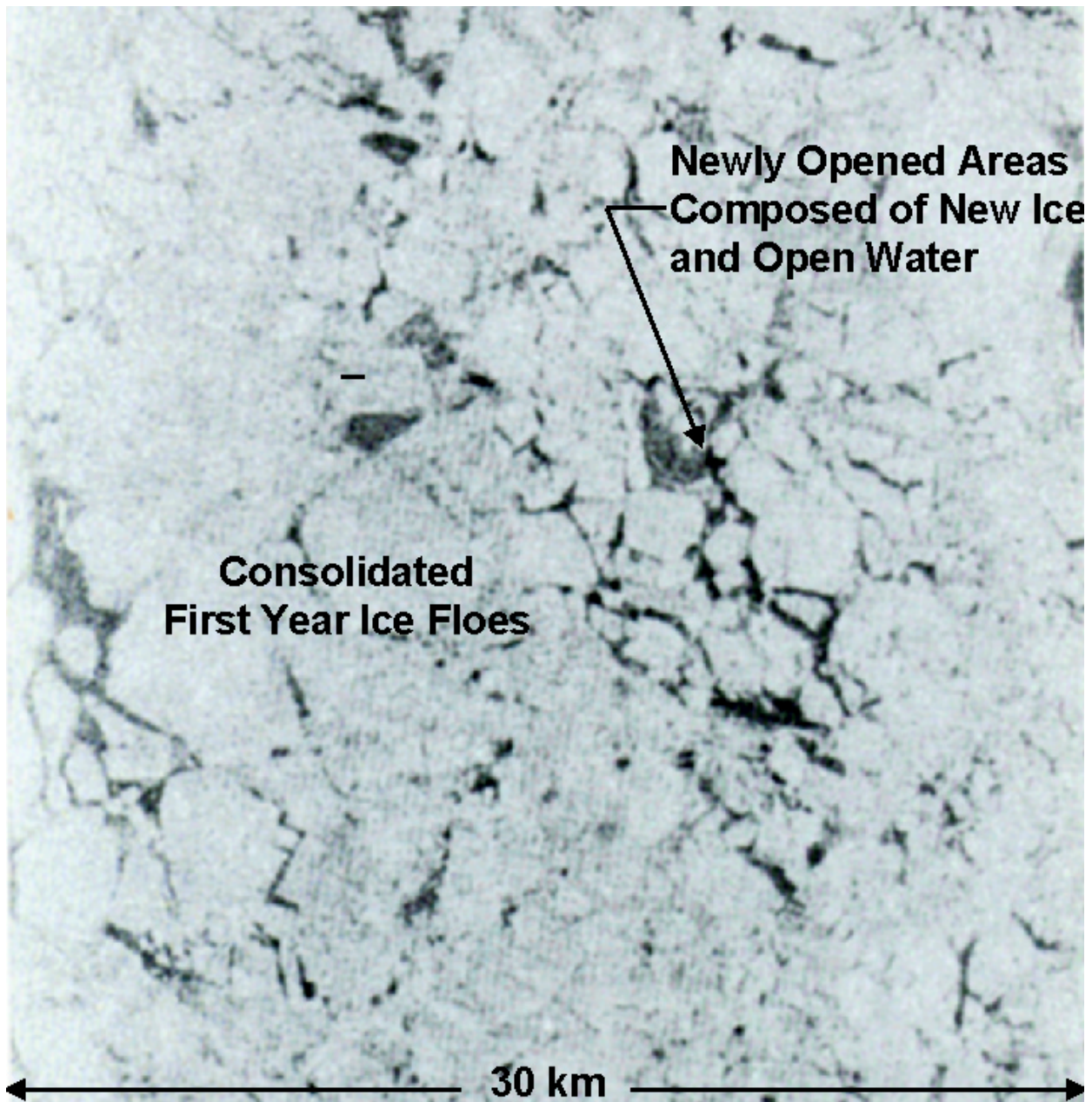


Figure 19.3. SIR-B (L-band HH) image of sea ice found in the Weddell Sea during October 1984. Dark areas are new ice and open water. Image location is 59°S 18°E.

#### 19.6.1 L-band Observations

L-band (e.g., frequency 1.25 GHz, wavelength 24 cm) imagery provides poor contrast between first-year and multiyear ice forms, but allows open water and new-young sea ice to be identified in a first-year / multiyear ice background. Small-scale surface roughness is not sufficient to be differentiated at this wavelength, and any volume scattering differences are minimized because this wavelength is too large compared to the small number of discrete scatterers (e.g., gas bubbles 1 mm in diameter) that are present in the ice fabric.

An area of marginal ice zone in the Scotia Sea as observed by SIR-B (L-band frequency, HH-polarization) in October 1984 is presented in Figure 19.2. The ground resolution for SIR-B is approximately 40 m x 40 m. Major features are regions several kilometers in size and most likely comprised of small pancakes with dark lead areas comprised of frazil. Pans and floes (i.e., 1 to 20 m in diameter) in the marginal ice zone are typically smaller than the resolution of the radar and produce a diffuse granular ice signature with no indication of floe boundaries. Pancake ice backscatter levels are large because of the many rough surface elements (e.g., pan rims) located within a resolution cell. Dark areas of weak backscatter may be found within regions of pancake ice. Due to the low signal-to-noise ratio of the SIR-B L-band data, it could not be determined if the dark areas represented new ice, streams of slush or frazil ice, or open water. The presence and presentation of frazil ice streams suggest the presence of local ocean surface currents. A discussion of the evolution of sea ice under wave action is found in *Onstott et al.*, [1998].

Analysis of additional imagery of this region indicated an ability to detect long surface gravity waves, icebergs, and the transition from small-to-large floes in the ice margin [*Carsey et al.*, 1986; *Martin et al.*, 1987]. Significant differences between the wet-ice/stormy-sea contrast at the ice edge and cold-ice/calm-sea conditions associated with leads farther into the pack were also observed. The sea ice returns were weaker than those of the ocean in this region, where the ocean is known to be rough.

Weddell Sea ice at its maximum thickness is shown in Figure 19.3 and was collected using SIR-B during October. Ice fracturing is clearly visible. The ice presentation shown in this image is typical of that found in the Weddell Sea, and is representative of ice conditions found in the Antarctic, in general. Note that floe boundaries are recognizable due to the delineation provided by the lower backscatter cross-sections of the open water and frazil ice even though SIR-B had a low signal-to-noise ratio. The new-ice/open-water found between the floes produces a weak backscatter. The presence of leads with weak backscatter indicates that the image was collected when the ice cover in this region was diverging [*Carsey et al.*, 1986, *Martin et al.*, 1987].

### 19.6.2 C-band Observations

C-band (i.e., frequency 5.25 GHz, wavelength 5.7 cm) SAR imagery provides good contrast between open water found in leads; new and young ice; smooth first-year ice; and rough, first-year and multiyear ice categories. This contrast is a result of higher operating frequency and finer resolution compared to L-band, which makes it more sensitive to differences in surface roughness and to the small discrete scatterers in the snow and upper ice layers.

Conditions in the early part of the Antarctic ice growth season are illustrated in the C-band image (RADARSAT-1) collected 26 April 1999 shown in Figure 19.4. The image includes the Ross Sea area about Ross Island, the McMurdo Sound, and the Ross Ice Shelf. The sea ice forms observed in this image are consolidated first-year ice (FY-C) which formed under dynamic conditions, ice which was sheltered and formed under quiescent conditions (FY-Q), and younger first-year ice which formed and was roughened during recent divergence events (FY-R). Note that there is a major lead that runs from the top of the image along the northwest side of Ross Island. The image also shows three glacial features of interest: an ice tongue (IT), an ice shelf, and a glacial ice stream (G). Also on the ice shelf is an ice runway (i.e., Williams Field) that is maintained by the U.S. McMurdo Station. Shelf and glacial ice produce a strong homogeneous backscatter response due to thick snow and firm layers. Ice tongues also have thick snow and firm

## Antarctic Sea Ice and Icebergs

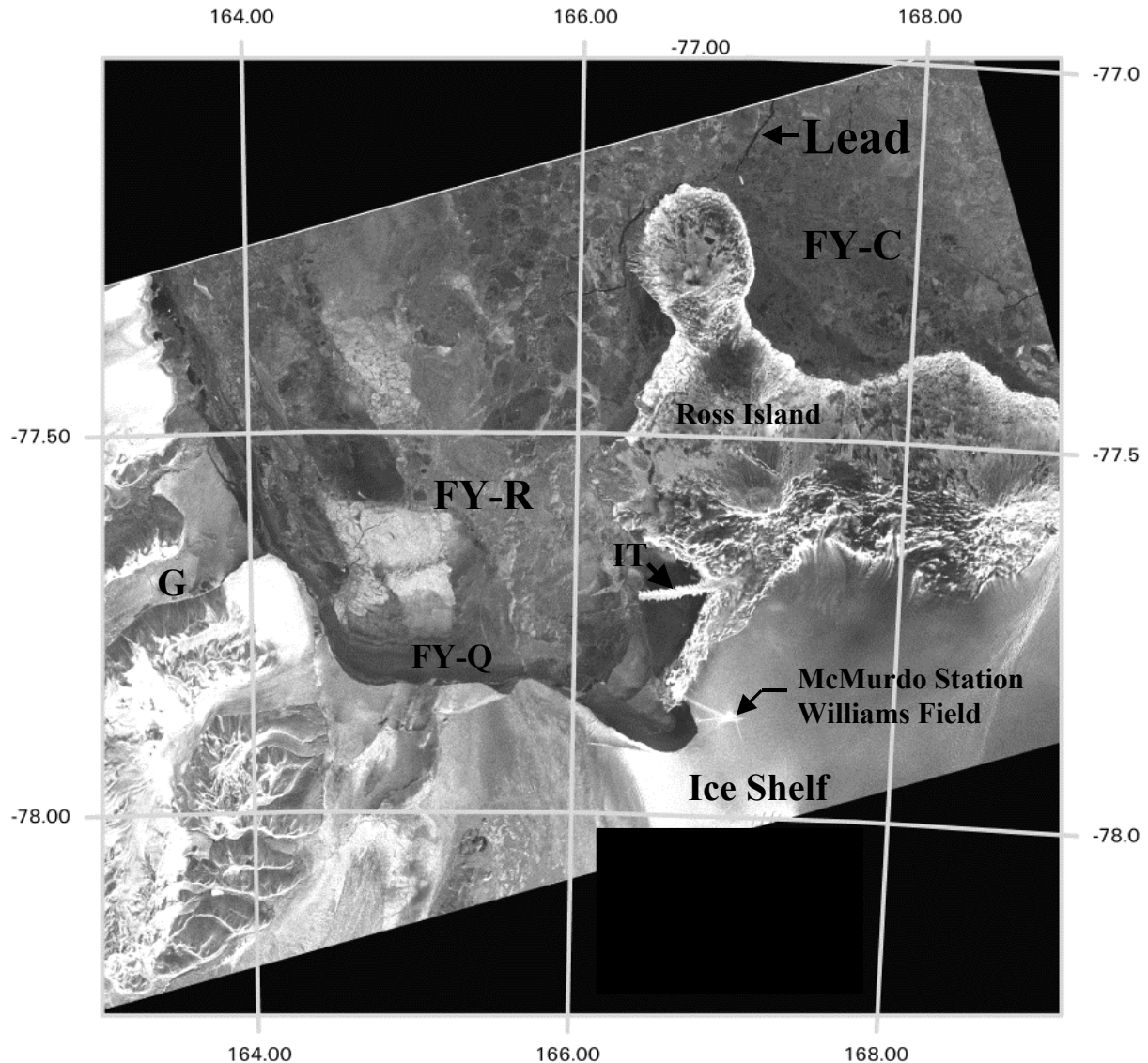


Figure 19.4. RADARSAT-1 (C-band, HH) image showing the region around Ross Island on 26 April 1999. Ice forms shown in this image include consolidated first year ice (FY-C), ice formed under quiescent conditions (FY-Q), rough young first year ice (FY-R), glacial ice tongue (IT), ice shelf (IS), and (c) glacial ice (G). The swath area is 100 km wide (N-S), with a range resolution of approximately 30 m. ©CSA 1999.

layers, and a large number of crevasses. Sea ice formed under quiescent conditions has a smooth snow-ice interface and produces a backscatter level that is weak when compared to ice with rough surfaces. The ice runway is an interesting feature in that it illustrates the effect that when snow is physically disturbed, in this case because of runway preparations, its backscatter may be enhanced.

To illustrate the rapid and dramatic change in sea ice conditions that occurs in the Antarctic during the early portion of the ice growth season, an image collected the following day (27 April 1999) is presented in Figure 19.5. During the period 26 to 27 April, katabatic winds attained an average speed of  $17.5 \text{ m s}^{-1}$ . This was sufficient to clear ice from McMurdo Sound. In the region cleared of consolidated ice, well-developed frazil ice streamers are observed in a dark region comprised of damped ocean water and rapidly forming new ice. The bright,

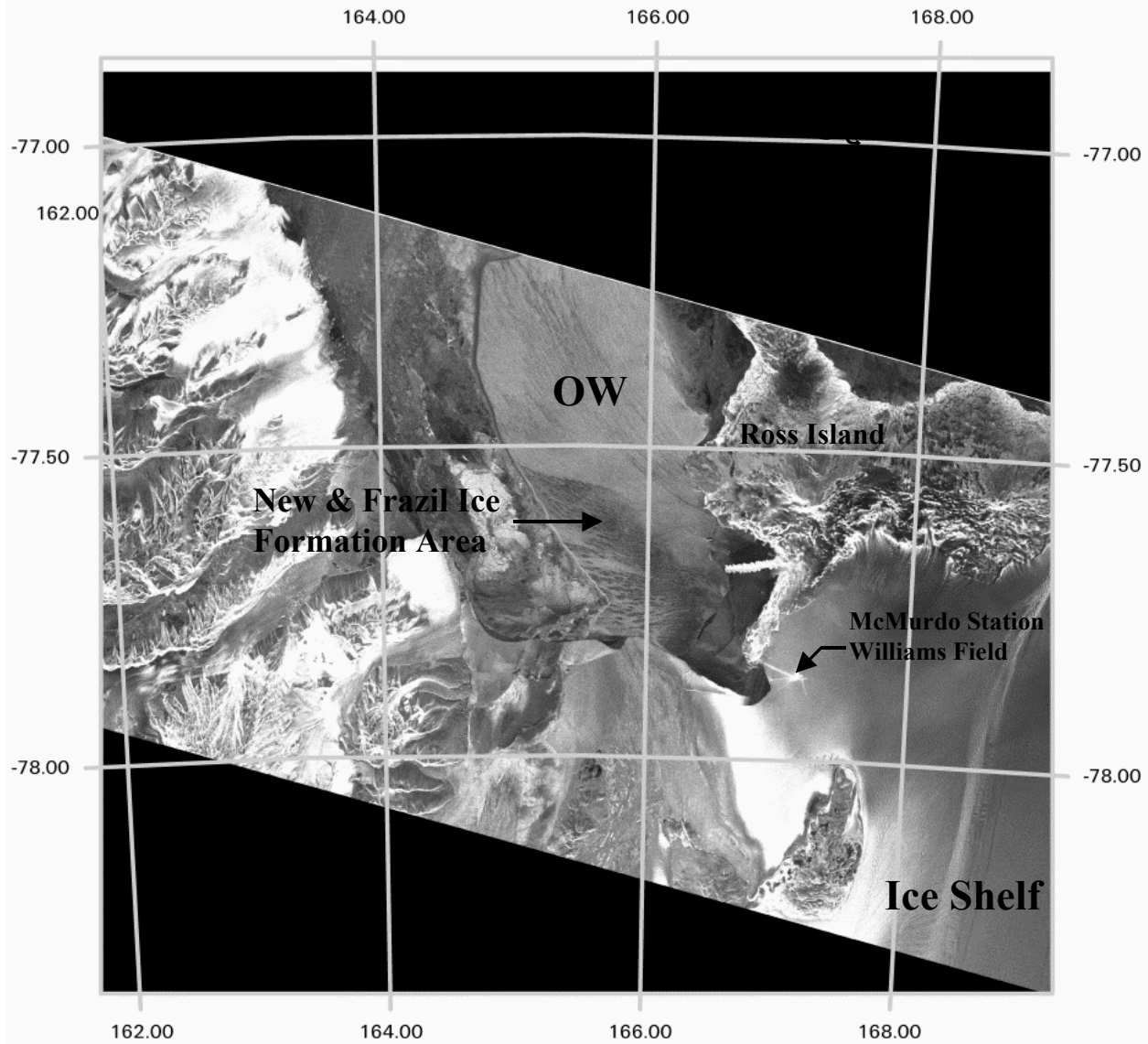


Figure 19-5. RADARSAT-1 (C-band, HH) image of the region around Ross Island on 27 April 1999 shows the presence of well-developed frazil ice streamers in a new ice production region and a zone of open water (OW). The swath area is 100 km wide. ©CSA 1999.

homogeneous region is open water (OW) driven by high winds. Dispersed frazil ice is expected to be present in the slightly less bright, long curvilinear features that are found oriented southeast to northwest.

Landfast ice, ice that is attached to the coastline, is illustrated in the C-band SAR image shown in Figure 19.6. As was observed in the Ross-Sea/McMurdo-Sound region over a three-year period (1997-1999) by the author, the ice that initially attaches to the coastline is not produced under quiescent conditions. Under calm winds, pans and cakes of ice consolidate into floes and thicken. Formation conditions, dominated by cycles of intense storms, produce landfast ice signatures that are moderately bright and spatially variable. The impact of strong katabatic winds on 2-month old first year ice is illustrated in Figure 19.6.

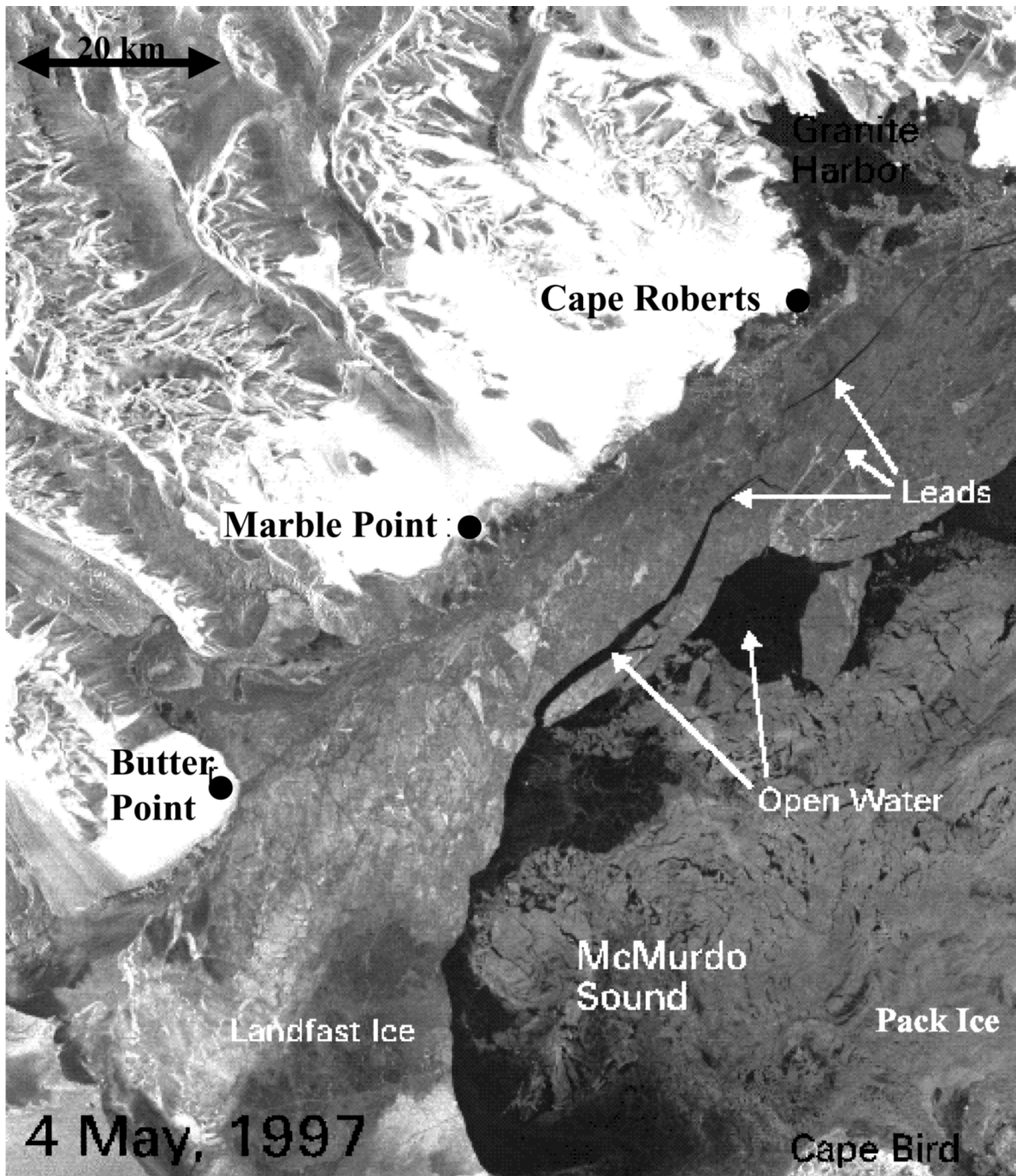


Figure 19.6. RADARSAT-1 (C-band, HH) image of the region near Cape Roberts (about 125 km from McMurdo Station at 77°02' S and 163°10' E) on 4 May 1997 after katabatic winds disturbed the previously consolidated young and landfast ice. © CSA, 1997.

In this case the stress due to strong katabatic winds (e.g., about  $10 \text{ m s}^{-1}$  for three days) causes the two-month old landfast ice to fail, forming numerous leads that follow the coastline. Because of the shadowing that the ice provides, the open water in these sheltered areas produces very weak backscatter at radar incident angles from  $20^\circ$  to  $50^\circ$ . The landfast ice is many tens of centimeters thick and forms moderate-to-large ice floes. The floating ice in McMurdo Sound

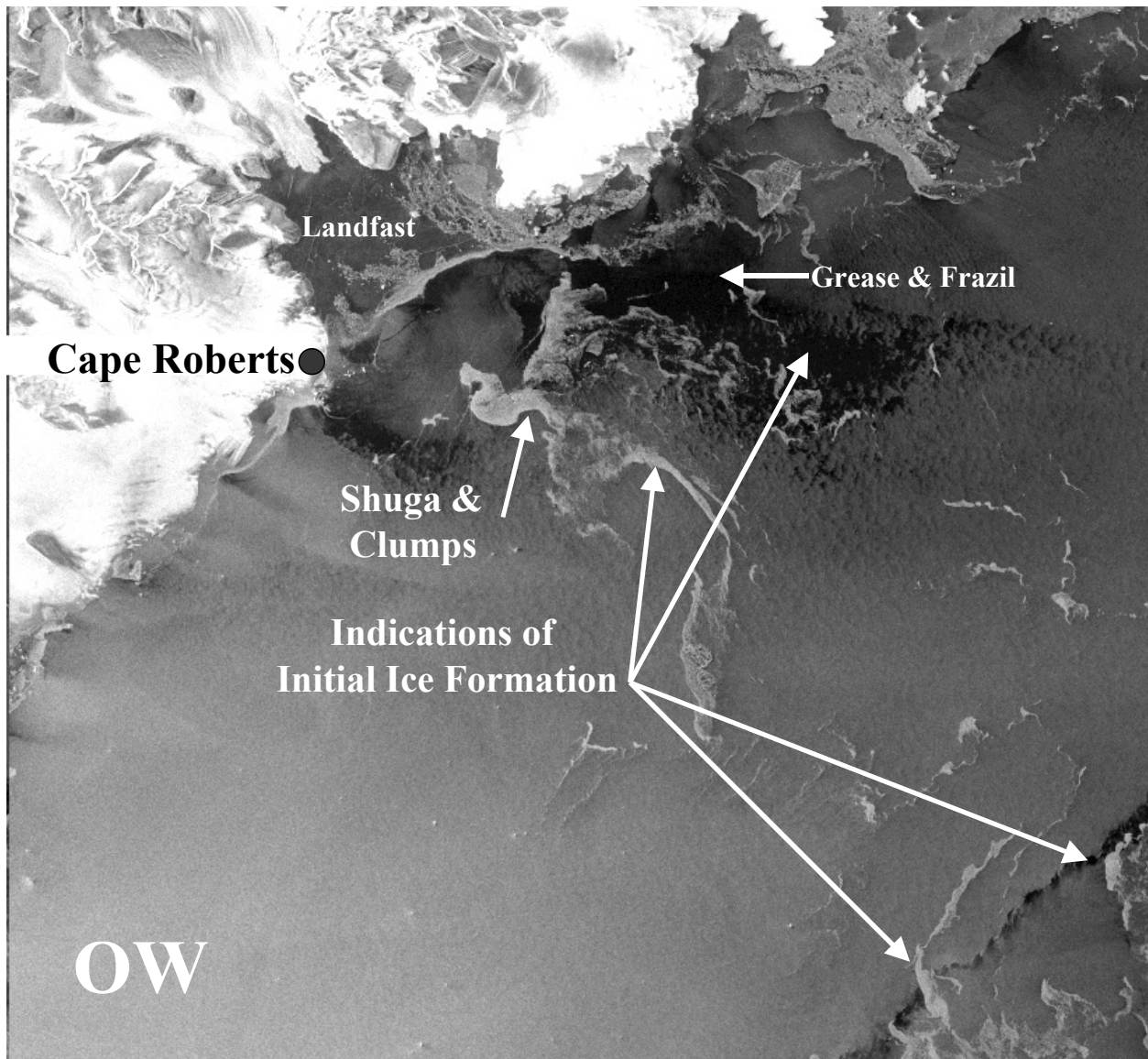


Figure 19.7. RADARSAT-1 (C-band, HH) image showing the coastal region near Cape Roberts on 3 February 1998. The imaged area is 100 km wide. ©CSA 1998

was thinner and easily broken into much smaller floes. New ice was produced in some of the open water areas and is detectable because of the rafting of new ice layers. Rafting produces a moderate increase in backscatter level where the rafts occur. As new ice ages, the backscatter also increases.

The detection of the initial ice formation is also important. In the Antarctic, air temperatures begin to drop by the end of January. A RADARSAT image of the Cape Roberts area was acquired on 3 February 1998 (see Figure 19.7) when air temperatures had reduced to about  $-12^{\circ}\text{C}$  and when wind speeds were 1 to  $7\text{ m s}^{-1}$  for a number of days. By 3 February, the upper ocean had cooled and the production of frazil ice had been initiated. The largely uniform appearance of the open water areas are highlighted by the presence of dark regions where grease and frazil ice are present, and bright areas where shuga or small pans have congregated into bands and streamers.

## Antarctic Sea Ice and Icebergs

### 19.6.3 X-band Observations

Limited amounts of X-Band SAR imagery were collected over the Marginal Ice Zone during the SIR-C/X-SAR mission in October 1994. The data were taken near the northern sea ice limit in the Weddell Sea and shows the ice edge, as well as pans, floes, and leads. The images appear similar in information content to the C-band imagery that were acquired at the same time.

## 19.7 Observation of Icebergs

Blocks of ice periodically “calve” from glacial ice tongues. Occasionally entire tongues break from the source glacier, or there may be a disintegration of a portion of ice shelf and produce “state” sized icebergs. Glaciers form in regions where temperatures are cold, snow accumulates over long time periods, and summer melt is limited. With time, recently fallen snow transforms into large granular ice crystals (e.g., firn). If snow accumulates yearly, the weight of the snow and firn compresses the material below (e.g., after a depth of about 60 m) into a body of solid, high-density ice. When a critical mass is attained, glaciers begin to flow, either due to a combination of gravity and pressure effects near the ice bedrock interface that cause plastic deformation, or due to deformation when the glacier is frozen to the bedrock. In the Antarctic, glaciers flow down from high altitudes outward toward sea level. Once they reach the ocean, a variety of forces cause failure of the glacial ice, and icebergs are born.

Icebergs are categorized according to size and shape. Size categories include (a) growler (0-5 m), (b) bergy bit (5-15 m), (c) small berg (15-60 m), (d) medium berg (60-120 m), (e) large berg (120-220 m), and very large bergs (> 220 m). Major shape categories include: (a) tabular, (b) non-tabular, (c) blocky, (d) wedge, (e) dry dock, and (f) pinnacle.

Some icebergs are so large that they become famous, or are involved in mishaps of great notoriety, such as the iceberg that the RMS Titanic struck. One recent well-publicized example of a giant iceberg is referred to as B-10A. Its original size was measured to be 39 km x 77 km. The source of the berg was determined to be the Thwaites Glacier that flows into the Amundsen Sea. It began as part of an even larger parent iceberg named B-10 that broke free in 1992. B-10 was tracked because it entered the southern shipping lanes and became a primary shipping hazard. The B-10A iceberg had an estimated height of 90 m above sea level, an estimated depth of 300 m, and a drift speed of 11 to 15 km/day. The National Ice Center (NIC) has the responsibility to provide worldwide operational analysis and forecasting of sea ice conditions and marine hazards, such as southern hemisphere icebergs. NIC first began tracking B-10 during January 1992. The primary sensor used to track icebergs at the NIC is the Defense Meteorological Satellite Program Operational Linescan System. Imagery is acquired in 3000 km-wide scans. Visible and IR data pixels are 550 m, nominally. In the summer of 1995, the B-10 iceberg broke into two pieces; the largest named B-10A. The smaller iceberg B-10B drifted west in and along the Antarctic ice pack and eventually became too small to warrant tracking in -10A, the larger fragment drifted east into the shipping lanes of the Drake Passage before becoming too small to track in spring of 2000.

During this period, observations of the giant iceberg were made using RADARSAT (see Figure 19.8a). B-10A moved well away from the Amundsen Sea and into rough open water. At a 5.7 cm radar wavelength (C-band), strong backscatter is produced by the very thick snow and firn layers, and numerous crevasses. Backscatter levels are sufficiently high that icebergs the size of B-10A are very easy to detect, no matter what the sea state. Icebergs one km in size are

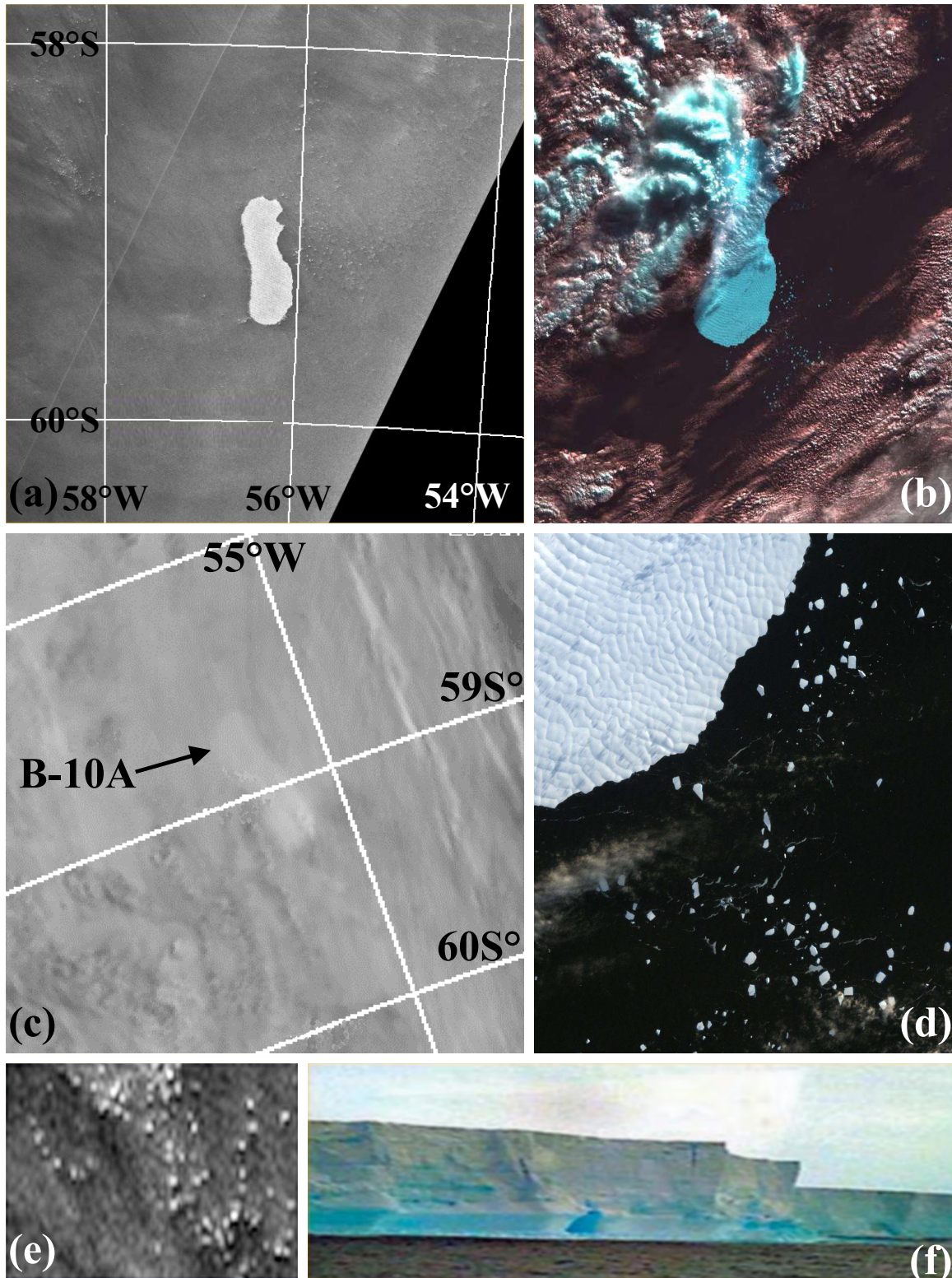


Figure 19.8. Giant iceberg was observed by RADARSAT-1 (C -band, HH) in August 1999. ©CSA 1999 (a), LANDSAT August 1999 (b), AVHRR-Visible October 1999 (c), calving shown by zooming in the LANDSAT image (d), SAR response of kilometer-sized icebergs (e), and surface level photo with credit to Mr. Keith Fenwick, UK Met Office, Falkland Islands (f). Images are courtesy of the National Ice Center.

## Antarctic Sea Ice and Icebergs

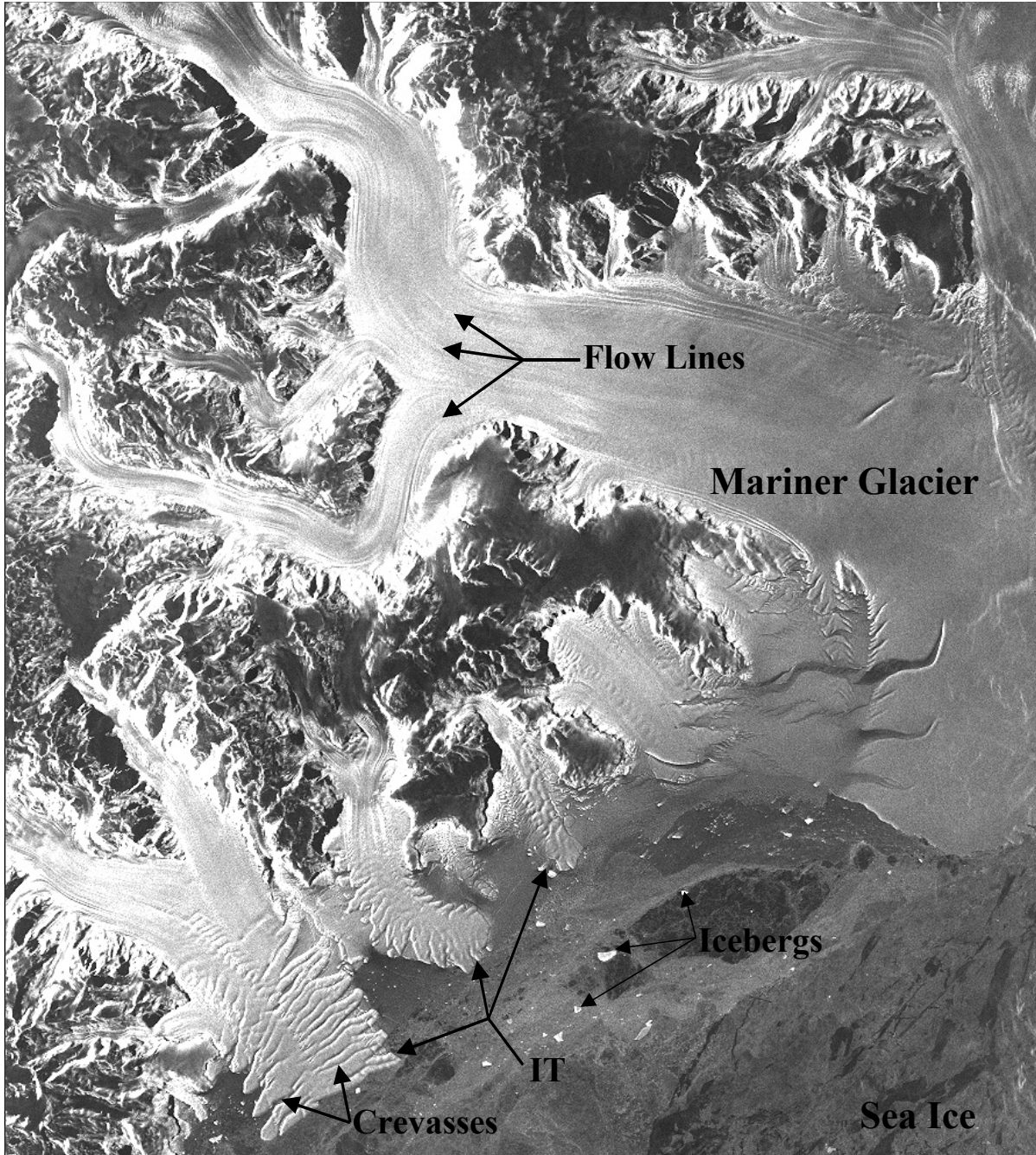


Figure 19.9. RADARSAT-1 (C-band, HH) image acquired on 4 October 1997 of the Mariner Glacier, Victoria Land ( $73^{\circ}10'S$  and  $166^{\circ}42' E$ ). The imaged area is 100-km x 100-km. ©CSA 1997.

more challenging, but are often first detected because multiple icebergs of kilometer size calve at the same time, drift together with similar velocities, and form a cluster of bergs in a relatively small area (see Figure 19.8e). In addition to a number of resolution cells that have a uniformly high backscatter level, there is the possibility of a shadow signature associated with the bright return (see Figure 19.8e). The shadow will increase with increasing incident angle, making radars that operate at the middle incident angles ( $30^{\circ}$ - $55^{\circ}$ ), such as RADARSAT, more optimum for iceberg detection.

LANDSAT-7 imagery can produce spectacular views of icebergs. Setting bands 5, 4, and 3 to red, green, and blue, respectively, maps the ice to blue-white, high clouds to white, low fog to greys and browns, and water to black, and is used to produce the image shown in Figure 19.8b. An AVHRR-Visible image is shown in Figure 19.8c. As is illustrated, detection of large, white icebergs is best when the background is a dark ocean. Cloud cover may become severe enough to prevent detection. Giant icebergs spawn numerous icebergs of one kilometer in size as illustrated in Figures 19.8b, 19.8d, and 19.8e. The photograph shown in Figure 19.8f suggests the massive size of this iceberg. Once icebergs enter the shipping zone of warm water, their lifespan rarely exceeds one year.

SAR imagery of Antarctic glaciers is spectacular as illustrated in the imagery of the Mariner Glacier in Northern Victoria Land (see Figure 19.9). Features of interest in this image are the glaciers that flow toward and beyond the coastline into the sea-ice covered Ross Sea. The glacial ice form called ice tongues is illustrated in the first three glaciers going from the bottom left hand corner following the coastline. Note that these ice tongues are structurally weak if they extend many kilometers away from the coastline and have well-developed crevasses. Periodic failure along the crevasses allows ice tongue segments to drift free as icebergs. Ice stream flow rates at their terminus may, at the extreme, reach velocities of  $1500 \text{ m yr}^{-1}$ . Also note that the backscatter from the ice tongues is much greater than that of sea ice. This allows for an easy detection of the numerous icebergs that are present in the coastal area. The largest icebergs in this image have a maximum dimension on the order of 2 to 3 km.

## 19.8 References

- Ackley, S. F., 1987: Mass balance aspects of Weddell Sea pack ice. CRREL Rep. 87-14, 70 pp.
- , A. J. Gow, K. R. Buck, and K. M. Golden, 1980: Sea ice studies in the Weddell Sea aboard USCGC Polar Sea. *Antarct. J. U.S.*, **15**, 84-86.
- Barry, R. G., 1989: The present climate of the Arctic Ocean and possible past and future states. *The Arctic Seas*, Y. Herman, Ed., Van Nostrand, 1-46.
- Carsey, F. D., B. Holt, S. Martin, L. McNutt, D. A. Rothrock, V. A. Squire, and W. F. Weeks, 1986: Weddell-Scotia Sea marginal ice zone observations from space, October 1984. *J. Geophys. Res.*, **91** (C3), 3920-3924.
- Drinkwater, M. R., 1998a: Active microwave remote sensing observations of Weddell Sea ice. *Antarctic Sea Ice: Physical Processes, Interactions and Variability*, M. O. Jeffries, Ed., Antarctic Research Series, Vol. 74, Amer. Geophys. Union, 187-212.
- , 1998b: Satellite microwave radar observations of Antarctic sea ice. *Analysis of SAR Data of the Polar Oceans, Recent Advances*, C. Tsatsoulis and R. Kwok, Eds., Springer, 145-187.
- , and V. Lytle, 1997: ERS-1 radar and field observed characteristics of autumn freeze-up in the Weddell Sea. *J. Geophys. Res.*, **102** (C6), 593-608.
- , and X. Liu, 2000: Seasonal to interannual variability in Antarctic sea-ice surface melt. *IEEE Trans. Geosci. Remote Sens.*, **38**, 1827-1842.
- Gloersen, P., W. J. Campbell, D. L. Cavalieri, J. C. Comiso, C. L. Parkinson, and H. J. Zwally, 1992: Arctic and Antarctic sea ice, 1978-1987: Satellite passive-microwave observations and analysis. National Aeronautics and Space Administration NASA SP-511, Washington DC, 290 pp.
- Gow, A. J., and W. B. Tucker III, 1990: Sea ice in the Polar regions. *Polar Oceanography, Part A, Physical Science*, W. O. Smith Jr., Ed., Academic Press, 47-122.

### Antarctic Sea Ice and Icebergs

- Lange, M. A., and H. Eicken, 1991: The sea ice thickness distributions in the Northwestern Weddell Sea, Antarctica. *J. Geophys. Res.*, **96**, 4821–4837.
- Lytle, V., and S. F. Ackley, 1991: Sea ice ridging in the eastern Weddell Sea. *J. Geophys. Res.*, **96**, 18 411–18 416.
- Martin, S., B. Holt, D. L. Cavalieri, and V. Squire, 1987: Shuttle imaging radar B (SIR-B) Weddell Sea ice observations: A comparison of SIR-B and scanning multichannel microwave radiometer sea ice concentrations. *J. Geophys. Res.*, **92** (C7), 7173–7179.
- Morris, K., M. O. Jeffries, and S. Li, 1998: Sea ice characteristics and seasonal variability of ERS-1 SAR backscatter in the Bellingshausen Sea. *Antarctic Sea Ice: Physical Processes, Interactions and Variability*, M. O. Jeffries, Ed., Antarctic Research Series, No. 74, Amer. Geophys. Union, 213–242.
- Onstott, R. G., P. Gogineni, A. J. Gow, T. C. Grenfell, K. C. Jezek, D. K. Perovich, and C. T. Swift, 1998: Electromagnetic and physical properties of sea ice formed in the presence of wave action. *IEEE Trans. Geosci. Remote Sens.*, **36B**, 1764–1783.
- Wadhams, P., M. A. Lange, and S. F. Ackley, 1987: The ice thickness distribution across the Atlantic sector of the Antarctic Ocean in midwinter. *J. Geophys. Res.*, **92**, 535–552.
- Weeks, W. F., S. F. Ackley, and J. W. Govoni, 1998: Sea ice ridging in the Ross Sea, Antarctica, as compared with sites in the Arctic. *J. Geophys. Res.*, **94**, 4984–4988.
- Zwally, H. J., J. C. Comiso, C. L. Parkinson, W. J. Campbell, F. D. Carsey, and P. Gloersen, 1983: Antarctic Sea Ice, 1973–1976—Satellite Passive-Microwave Observations, National Aeronautics and Space Administration NASA SP-459, Washington, DC, 206 pp.